



Impact of the electron beam on the thermal stability of gold nanorods studied by environmental transmission electron microscopy

Wiebke Albrecht^a, Arjen van de Glind^b, Hideto Yoshida^c, Yusuke Isozaki^{c,d}, Arnout Imhof^a, Alfons van Blaaderen^a, Petra E. de Jongh^b, Krijn P. de Jong^b, Jovana Zečević^{*,b}, Seiji Takeda^{c,*}

^a Soft Condensed Matter, Debye Institute for Nanomaterials Science, Utrecht University, Princetonplein 5, Utrecht 3584 CC, The Netherlands

^b Inorganic Chemistry and Catalysis, Debye Institute for Nanomaterials Science, Utrecht University, Universiteitsweg 99, Utrecht 3584 CG, The Netherlands

^c The Institute of Scientific and Industrial Research, Osaka University, 8-1 Mihogaoka, Ibaraki, Osaka 567-0047, Japan

^d Division of Materials and Manufacturing Science, Graduate School of Engineering, Osaka University, 2-1 Yamadaoka, Suita, Osaka 565-0871, Japan

ARTICLE INFO

Keywords:

Environmental transmission electron microscopy
Gold
Nanoparticles
Thermal stability
Electron beam effects

ABSTRACT

In-situ transmission electron microscopy experiments are of great interest to nanoscience and nanotechnology. However, it is known that the electron beam can have a significant impact on the structure of the sample which makes it important to carefully interpret in-situ data. In this work, we studied the thermal stability of CTAB-stabilized gold nanorods under different gaseous environments in an environmental transmission electron microscope and compared the outcome to ex-situ heating experiments. We observed a remarkable influence of the electron beam: While the nanorods were stable under inert conditions when exposed to the electron beam even at 400°C, the same nanorods reshaped at temperatures as low as 100°C under ex-situ conditions. We ascribe the stabilizing effect to the transformation of the CTAB bi-layer into a thin carbon layer under electron beam irradiation, preventing the nanorods from deforming. When exposed to an oxidizing environment in the environmental transmission electron microscope, this carbon layer was gradually removed and the gold atoms became mobile allowing for the deformation of the rod. This work highlights the importance of understanding the phenomena taking place under electron beam irradiation, which can greatly affect in-situ experiments and conclusions drawn from these. It stresses that in-situ electron microscopy data, taken on measuring the temperature dependence of nanoparticle properties, should be carefully assessed and accompanied by ex-situ experiments if possible.

1. Introduction

When scaled down to nanometer size, many materials exhibit properties quite different from those of a bulk phase. This phenomenon has been the basis for the development of nanoscience and nanotechnology and has led to breakthroughs in various fields of research, ranging from physics and chemistry to medicine. In metal nanoparticles the confinement of electrons to the nanometer scale was found to result in exciting new phenomena. Among a plethora of different shapes and metals, gold nanorods (Au NRs) attracted a lot of scientific attention. Due to their tunable optical properties, catalytic activity, high chemical stability and bio-compatibility, Au NRs are considered for a wide variety of applications like drug delivery [1,2], sensing [3–6], photocatalysis [7], data storage [8–11] and hyperthermic cancer treatment [2,12–14].

Localized surface plasmon resonances (LSPRs) lie at the core of many applications as they lead to strong local electric field

enhancements, especially at sharp corners and tips. Due to their anisotropic shape, Au NRs exhibit a (degenerated) transverse and a longitudinal LSPR. While the transverse resonance has a wavelength around 520 nm, the longitudinal LSPR can be tuned from the near-infrared to the visible part of the electromagnetic spectrum by decreasing the aspect ratio of the NR [15,16]. Thus, understanding the thermal stability of Au NRs is of crucial importance since a heat-induced deformation of the NRs leads to a decrease in aspect ratio and consequently affects their optical properties [17–19]. It is generally established that the NR shape becomes unstable upon heating to temperatures many hundreds of degrees below the bulk melting temperature (1064°C), sometimes even as low as 100°C [20,21]. The thermal stability can be enhanced by an inorganic, possibly mesoporous, coating such as silica that hinders the diffusion of surface atoms [22–25]. Despite the increasing interest in anisotropic NPs as (photo)catalysts for oxidation and hydrogenation reactions, to the best of our knowledge, no extensive research has been performed to study their thermal stability under different gaseous

* Corresponding authors.

E-mail addresses: J.Zečević@uu.nl (J. Zečević), takeda@sanken.osaka-u.ac.jp (S. Takeda).

<https://doi.org/10.1016/j.ultramic.2018.05.006>

Received 17 October 2017; Received in revised form 13 April 2018; Accepted 29 May 2018

Available online 18 June 2018

0304-3991/ © 2018 The Authors. Published by Elsevier B.V. This is an open access article under the CC BY license (<http://creativecommons.org/licenses/by/4.0/>).

environments and thus more realistic catalytic conditions.

Transmission electron microscopy (TEM) has played a pivotal role in investigating nanomaterials' structures and linking properties associated with the nano length scale(s) of materials to their bulk behavior. Furthermore, the development of environmental TEM (ETEM), with gaseous environments in the sample chamber and heating elements, allows for various experiments to be performed in-situ, revealing sample transformations in real time and under a wider range of conditions [26–29]. In addition, we chose ETEM for studying the thermal stability of Au NRs in different environments. However, when choosing an electron-beam technique, one challenge is to understand and/or minimize the influence of the electron beam on the measurements.

In recent years, more attention has been drawn to the potentially strong effects that the electron beam can have on the processes studied in-situ (E)TEM investigations. Apart from well-known e-beam induced damages to the sample's structure during regular TEM imaging [30], in-situ TEM studies with or without heating under vacuum, gas-phase and liquid phase conditions, brought about additional challenges. It was recently shown, for example, that the electron beam leads to an increased dislocation activation during in-situ TEM experiments investigating tensile straining of aluminum and gold films [31]. Furthermore, the electron beam ionizes gas molecules which can lead to an increased reactivity, as seen for the oxidation of carbon nanotubes [32] and Pt nanoparticles [33] observed by ETEM. In the case of the recently developed liquid phase TEM, the electron beam effects are perhaps the most prominent, as it was repeatedly argued that the electron beam leads to radiolysis of water and a formation of various reducing and oxidizing species [34]. Therefore, it is ever more important to carefully assess the impact of the electron beam on the samples' behavior.

In our experiments, we observed that the electron beam significantly increased the thermal stability of Au NRs, through the formation of a protective carbon layer formed almost instantly by high-energy electron beam induced pyrolysis of the organic surfactant surrounding the Au NRs. Owing to the use of an ETEM, an oxidizing environment could be introduced which led to the gradual removal of the carbon layer. Our research shows that an electron beam and the presence or absence of certain gasses can have a large impact on a sample during in-situ TEM experiments and calls for critical assessment of in-situ TEM data and a need for comparison with ex-situ experiments before any conclusions about the sample structure and/or behavior can be drawn.

2. Experimental

2.1. Synthesis of Au NRs

The following chemicals were used: gold(III) chloride trihydrate (99,9%, CAS nr: 16961-25-4), cetyltrimethylammonium bromide (98%, CAS nr: 57-09-0) and L-ascorbic acid (99%, CAS nr: 50-81-7) from Sigma Aldrich. Sodium borohydride (98%, CAS nr: 16961-66-2) and silver nitrate (99,9%, CAS nr: 7761-88-8) were purchased from Alfa Aesar. All synthesis steps were performed using purified Milli-Q water (Merck, 18.2 M Ω).

The Au NRs were grown via a silver-assisted seeded growth method described by Liz Marzán et al. [35]. This method consists of preparing the growth solution and the gold seeds separately before adding the seeds as nuclei to the growth solution. First the gold seeds were synthesized by preparing 10 mL of an aqueous solution containing 0.25 mM HAuCl₄ and 0.1 M cetyltrimethylammoniumbromide (CTAB). Successively the solution was vigorously stirred at room temperature, while 0.6 mL of freshly prepared 10 mM NaBH₄ solution was added. The reaction mixture was stirred for 2 minutes and aged for 5–10 minutes before further use. Second, 500 mL of the aqueous growth solution containing 0.5 mM HAuCl₄, 0.1 M CTAB, and 0.12 mM AgNO₃ was prepared. Then the solution was brought to pH 3–3.5 by addition of HCl. Throughout the synthesis the solution was stirred gently at 30 °C.

In order to reduce the gold, 3.5 mL of 78.8 mM ascorbic acid was added, followed by the addition of 0.6 mL freshly prepared gold seeds. The reaction mixture was gently stirred overnight.

To grow the Au NRs larger than reported by Liz Marzán et al. [35] more reducing agent was added in 5 successive steps with a 2 h interval. In each step 0.31 mL of 78.8 mM ascorbic acid was added and the reaction mixture was again gently stirred overnight. The mixture was then washed twice by centrifugation at 6500 RPM for 1 h. In order to prevent aggregation of the NRs, the CTAB concentration was kept at 8 mM. The average length and width of the obtained NRs were 64.5 nm and 18.6 nm, respectively.

2.2. Ex-situ heating experiments

Two consecutive droplets (the second one was placed after evaporation of the first drop) of the Au NRs' solution were dried on microscope glass slides (76 × 26 mm, Thermo scientific, Menzel-Gläser) and placed in a preheated static air oven (Carbolite) at either 100°, 150°C or 200°C for one hour. The extinction of the heated NRs on the microscope slide was measured with an empty glass slide as reference. The extinction measurements were performed on a Bruker Vertex 70 FT VIS-IR spectrometer. The Au NRs were then redispersed in H₂O before placement on a TEM grid. The TEM measurements of the ex-situ treated samples were performed on a FEI Tecnai 12 microscope operated at 120 kV.

2.3. In-situ heating experiments

For the experiments in vacuum, a drop of the CTAB-coated Au NRs dispersion was dried on a TEM heating chip consisting of several silicon nitride windows surrounded by a coiled Pt wire. The TEM heating chip was then placed in a DENS solutions heating holder and heated resistively in-situ to 400°C by increasing the temperature by 50°C every 20 s. The TEM imaging in this experiment was performed with a FEI Tecnai 12 microscope operated at 120 kV. During the heating to 400°C and during 1 h at that temperature one selected window of the heating chip was exposed to the electron beam, while other areas were imaged afterwards.

For the ETEM experiments, the Au NRs samples were supported on a Mo grid mesh with a holey carbon supporting film. A mesh with deposited NRs was fixed onto a TEM heating holder and transferred to an ETEM (FEI Tecnai F20 transmission electron microscope equipped with a specially designed environmental cell [36]) operated at 200 kV. Gaseous O₂, N₂, CO, and mixtures of these gases were introduced into the environmental cell and the samples were observed at room temperature, at 100°C, 200°C, 300°C, and at 400°C. The heating rate of the sample was 10°C min⁻¹. ETEM observations were started 60 minutes after reaching the target temperatures. The nominal impurities in all the gases were less than 0.005 vol%. Residual gases in the ETEM were measured using a quadrupole mass spectrometer. The total pressure of residual gas was about 6.5·10⁻² Pa, of which the partial pressures of constituent gases were H₂O: 5.9·10⁻² Pa, N₂: 0.3·10⁻² Pa, O₂: 0.2·10⁻² Pa, and CO₂: 0.1·10⁻² Pa. For the ETEM experiments performed on the Au NRs, the pressure of different gases was varied between 50 Pa and 200 Pa to ensure that the pressure is much higher than that of the residual gases and vacuum. We also observed the NRs under vacuum at the above mentioned temperatures in the ETEM. ETEM images were acquired using small electron beam currents lower than 1.0 Acm⁻². High resolution TEM images were obtained by a Titan ETEM G2 (FEI) operated at 300 kV.

Energy dispersive X-ray analysis was performed on a JEM-ARM200F (JEOL) microscope operated at 200 kV. Electron energy-loss spectroscopy was performed on a Titan ETEM G2 (FEI) microscope operated at 80 kV.

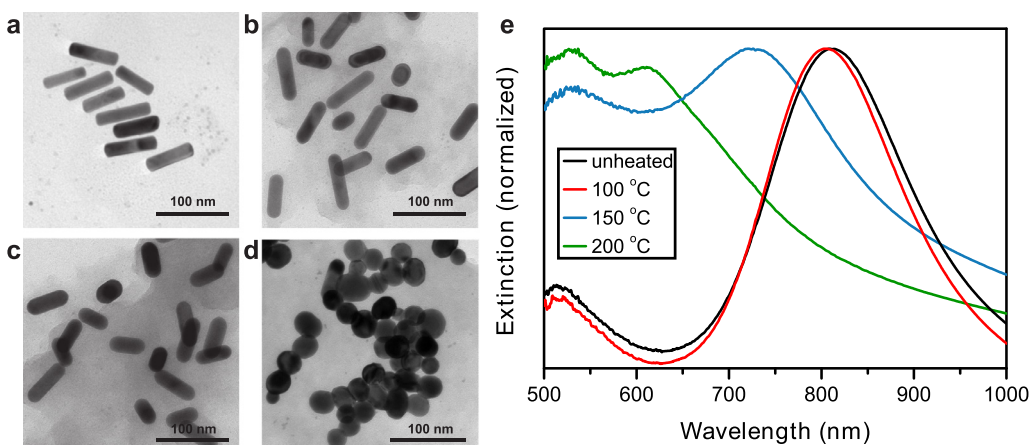


Fig. 1. TEM images of Au NRs after ex-situ heat treatments in air. a) Freshly prepared Au NRs drop-casted on a TEM grid and dried at ambient conditions having an average aspect ratio of 3.5. After heating at 100°C for 1 h in air (b) a fraction of the Au NRs deformed, resulting in a reduction of the average aspect ratio from 3.5 to 3.1. Upon heating at 150°C for 1 h (c) the average aspect ratio of the Au NRs further decreased to 1.7. After 1 h of heating in air at 200°C (d) almost complete deformation to a spherical shape with an average aspect ratio of 1.2 and sintering was observed. The particles were re-dispersed in water after thermal treatment to enable drop-casting on a TEM grid. (e) Extinction spectra of the un-

heated and heated NRs deposited on a microscope slide show a clear deformation towards a spherical shape indicated by the blue-shift of the longitudinal plasmon peak. After heating at 200°C for one hour the longitudinal plasmon peak almost coincides with the transverse one at 520 nm indicating that all particles were nearly fully deformed. (For interpretation of the references to colour in this figure legend, the reader is referred to the web version of this article.)

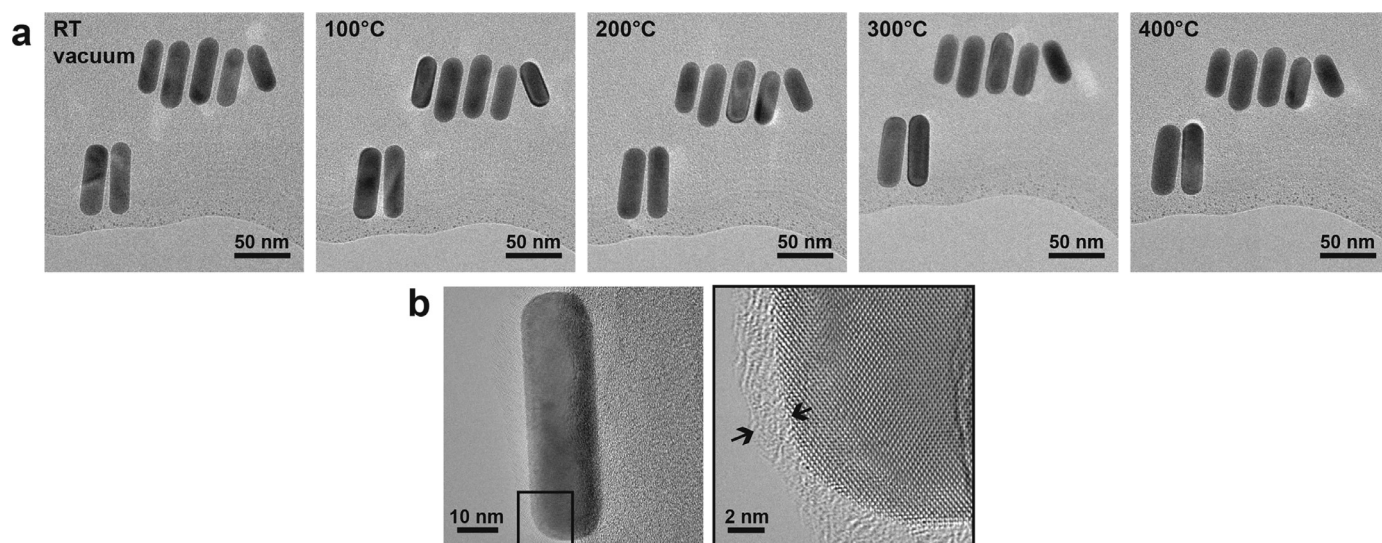


Fig. 2. ETEM images of Au NRs in-situ heat treated to 400°C with steps of 100°C under vacuum (a). Each image was taken after one hour dwell time at the given temperature. High resolution TEM image taken at RT indicating the presence of a 2 nm thick carbon layer around the Au particles (b).

3. Results and discussion

In order to investigate their thermal stability, we first heated Au NRs with an average aspect ratio of 3.5 (average length = 64.5 nm, average width = 18.6 nm) ex-situ in a preheated static air oven at either 100°C, 150°C or 200°C for 1 h on a glass substrate. After heating we redispersed the heated particles in water and we dropcasted the obtained solutions on a TEM grid for further analysis. TEM images of the unheated and heated NRs are shown in Figs. 1a and 1 b-d, respectively. An average aspect ratio was determined by measuring the length and width of at least 50 particles. Already after being heated for one hour at 100°C the average aspect ratio of the Au NRs decreased to 3.1, while after one hour at 150°C the average aspect ratio of the Au NRs dropped to 1.7. When the sample was heated at 200°C for 1 h, the Au NRs lost their anisotropic shape almost completely by deforming to nearly spherical particles with an average aspect ratio of 1.2 and by sintering to large more or less spherical but still crystalline particles (Fig. 1d). Since CTAB is known to start decomposing at 200°C [37], part of the CTAB molecules surrounding the Au NRs might have decomposed making sintering of the NRs possible. However, it is likely that part of the CTAB was still present as the Au NRs could still be dispersed in water after heating on a

glass plate.

The TEM results were supported by extinction measurements (Fig. 1e) monitoring the shift of the longitudinal plasmon peak and thus the deformation of a much larger number of particles compared to the TEM measurements. The decreasing aspect ratio was confirmed by the shift of the longitudinal plasmon peak to lower wavelengths upon heating (Fig. 1e). For the NRs that were heated at 100°C only a small blue-shift from 812 nm to 805 nm occurred in agreement with a small decrease in aspect ratio to 3.1 as observed by TEM. After heating at 150°C the longitudinal surface plasmon peak further blue-shifted to 726 nm which is in agreement with the observed decrease in aspect ratio to 1.7 obtained from the TEM images. The deformation to nearly spherical particles after heating at 200°C for 1 h is also seen in the extinction spectrum where the longitudinal peak shifted to 610 nm. For perfectly spherical particles the longitudinal resonance should be at the same resonance as the transverse ones located at 520 nm. As can be seen from Fig. 1d, many particles are still slightly anisotropic and/or partially sintered. Both cases lead to a red-shifted resonance as observed in Fig. 1e. It needs to be mentioned that the peak positions are also influenced by the close proximity (less than 10 nm) of the (un-sintered) NRs on the glass which can lead to coupling and consequently

to a further red-shift of the resonance.

In an attempt to understand the kinetics of the thermally induced deformations and the dependence on conditions at which the heating was performed, we continued our experiments with in-situ measurements in an ETEM under vacuum conditions. Fig. 2 shows the TEM images of Au NRs supported on a holey carbon film and heated in-situ under vacuum with a heating rate of $10^{\circ}\text{C min}^{-1}$. Images were taken after 1 h of heating at 100°C , 200°C , 300°C and finally 400°C . To our surprise, the same NRs that completely deformed after 1 h of ex-situ heating at 200°C , barely deformed in the electron microscope even after heating at 400°C for 1 h. Additional experiments performed at higher magnification revealed that a 2 nm thin layer of carbon surrounded the Au NR already at room temperature (Fig. 2b, see Supporting Figure S1 for high resolution images at higher temperatures). This thickness is of the same order as the 3 nm thick bi-layer of CTAB which is expected to be on the Au NRs surface [38]. It is likely that upon electron beam irradiation, the CTAB layer around the Au NRs was transformed almost instantly into an amorphous carbon layer, through the process of pyrolysis, as it is known from literature that hydrocarbon species easily fragment and carbonize by electron beam irradiation [39]. Both electron energy-loss spectroscopy (EELS) and energy dispersive X-ray (EDX) analysis showed that the thin layer on the surface of the Au NRs consisted of carbon after TEM observation in vacuum and at room temperature (Fig. 3 and Supporting Figure S2).

Since the TEM support for the experiments shown in Fig. 2 contained a holey carbon film it cannot be concluded that the electron beam induced carbon layer solely arose from the transformation of CTAB, as the holey carbon film could act as a carbon source as well. Thus, we performed additional experiments in which a heating chip with silicon nitride electron transparent windows was used as a support for the Au NRs, instead of a holey carbon film. Therefore, this limits the amount of carbon not originating from the CTAB layer around the Au

NRs, participated in the creation of the protective carbon layer. The results are presented in Fig. 4. Similarly to the previous experiment, the Au NRs barely deformed even after heating at 400°C for one hour (Fig. 4a). However, the NRs located at other areas of the heating chip, which were not irradiated by the electron beam prior to and during the heating, completely deformed to spherical shapes (Fig. 4b), which is in agreement with the ex-situ observations. We conclude that in the absence of the electron beam the unaffected CTAB on the surface was not able to prevent the Au particles from deforming (Fig. 4b). On the other hand, when CTAB was first exposed to the electron beam, it quickly transformed into an amorphous carbon layer that was apparently rigid enough, even being only a few nm thin, to prevent diffusion of metal atoms.

Based on the above findings, we anticipated that if the CTAB layer were removed, deformation of Au NRs would take place during in-situ TEM at the same temperatures as it occurred in the ex-situ heating experiments. In an attempt to remove the CTAB layer, we plasma cleaned the Au NRs deposited on a silicon nitride heating chip for 20 min in a mixed O_2 and Ar atmosphere [40]. In-situ TEM heat treatment (using the same conditions as for Fig. 4) showed quite surprising effects: both electron beam irradiated and non-irradiated Au NRs retained their anisotropic character, and only slight sintering occurred when the Au NRs were close to each other (Supporting Figure S3). This suggests that instead of removing the CTAB, plasma cleaning under the conditions applied altered the CTABs structure into a protective layer similar to the electron beam induced amorphous carbon. It should be noted that 20 min of plasma cleaning is relatively long and does not necessarily mimic normal plasma cleaning conditions as carbon based grids are normally plasma cleaned for about 30 s. Thus, to fully address this phenomenon, additional experiments are required to find specific plasma cleaning conditions under which the CTAB layer is fully removed.

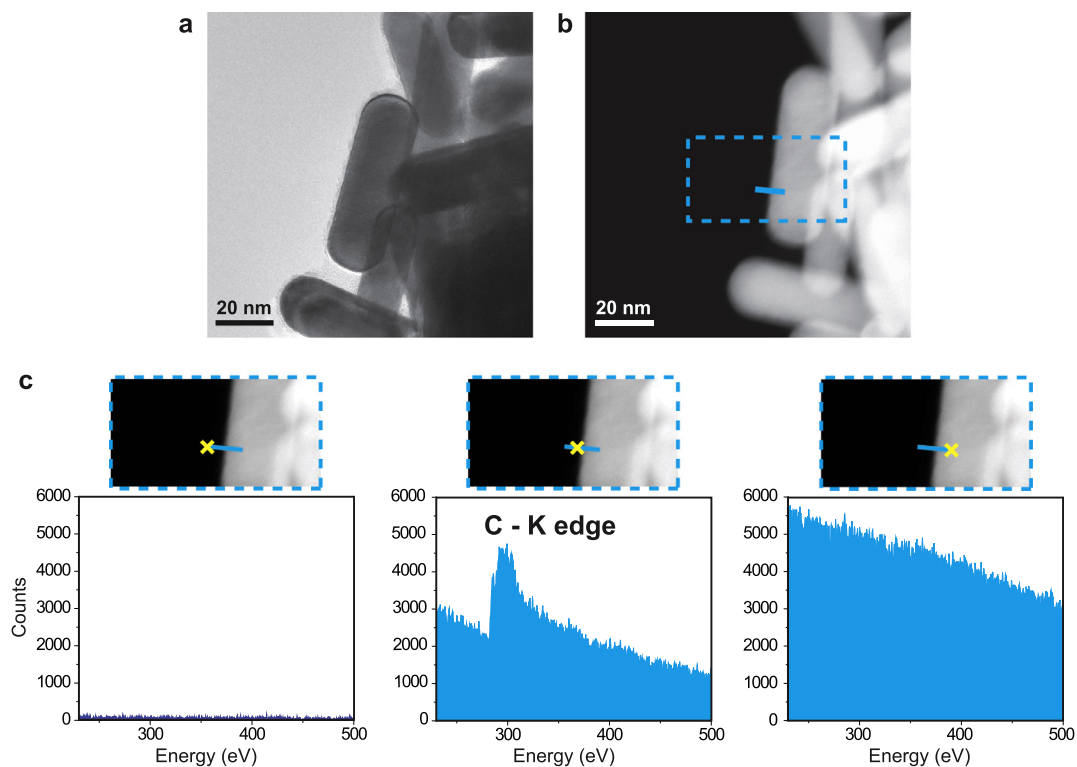


Fig. 3. Electron energy-loss spectroscopy (EELS) of Au NRs dispersed on a Cu grid with a holey carbon film. (a) and (b) exhibit the bright-field TEM image and dark-field STEM image, respectively, of Au NRs. The rectangle indicates the area in which the EELS line scan was taken (blue line). (c) EELS spectra of three different points along the line, clearly showing: the absence of any signal (left spectrum) several nanometers away from the Au NR, the presence of a carbon peak at the spot that is within 2–3 nm from the Au NR (middle spectrum) and the spectrum in which the nanometer peak is hidden in the background of an intense Au signal (right spectrum). (For interpretation of the references to colour in this figure legend, the reader is referred to the web version of this article.)

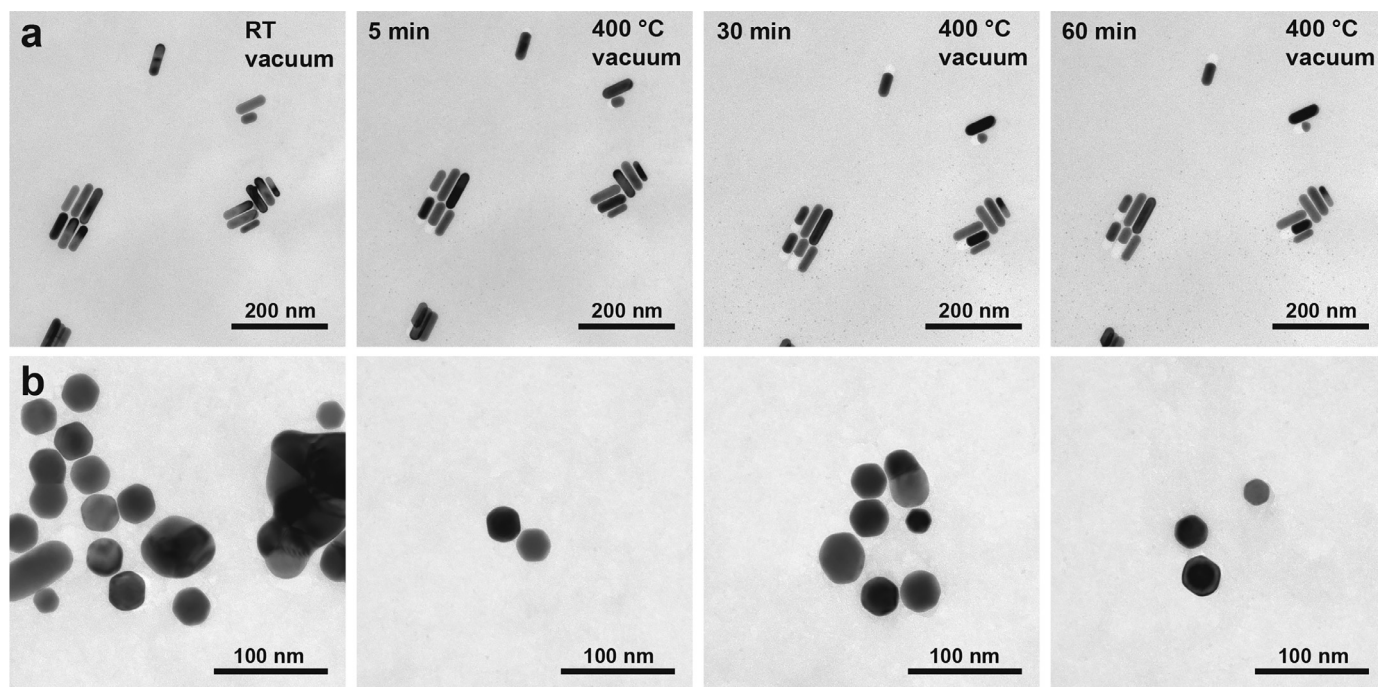


Fig. 4. Comparison of electron beam irradiated and non-irradiated Au NRs during in-situ TEM heating. (a) Au NRs imaged prior to heating, and after 5 min, 30 min and 60 min heating at 400°C in vacuum. The Au NRs were mostly stable, with only a slight deformation observed. (b) Several areas of the same heating chip that were not exposed to the electron beam prior to and during heating to 400°C, clearly showing complete deformation and even sintering of Au NRs.

The importance of a carbon coating on silver nanoparticles has also been recently recognized by Asoro et al. [41,42] who performed in-situ heating TEM measurements to study the sintering mechanism of spherical silver nanoparticles. They observed that the surface diffusivity of silver atoms during the sintering of two adjacent silver nanoparticles was decreased by two orders of magnitude in the presence of a carbon coating, which was either intentionally added or a remnant of the synthesis, compared to uncoated particles. As the heat-induced deformation of Au NRs is mainly driven by diffusion of the surface atoms [43], such a drastic reduction in diffusivity can explain why the carbon-coated NRs did not deform in our experiments up to heating temperatures of 400°C.

Our results can also help to understand discrepancies between the thermal stability observed under ex-situ conditions and in-situ electron microscopy experiments. For example, Petrova et al. found that PVP-stabilized Au NRs with an average AR = 3.3 (73 nm × 22 nm) completely deformed to a spherical shape after heating in an oven for 1 h at 250°C [21]. On the other hand, Khalavka and co-workers only observed conformational changes of a CTAB-stabilized Au NR after hours of heating at 380°C in an electron microscope [22]. While Petrovas' results agree well with our ex-situ heating experiments on our slightly smaller NRs (Fig. 1), Khalavkas' results are in agreement with our in-situ heating results. Thus, in their case the NRs were almost certainly stabilized by a carbon shell. While the authors noticed the occurrence of a graphitic shell around the NRs, they did not relate the formation of the graphitic shell to the electron beam but to the high heating temperature which can also graphitize organic residues. Our results show, however, that the electron beam is responsible for transforming the CTAB into a carbon layer and not the heating itself as the carbon shell was not observed for heated but unirradiated NRs (Fig. 4b).

Different gaseous environments are expected to influence the stability of the NRs therefore in different ways, a topic which is especially interesting for catalysis applications. Thus, we performed in-situ heating experiments in five different gaseous environments: N₂, CO and O₂ gas, as well as mixed N₂/O₂ (1:1) and CO/O₂ (1:1) atmospheres, and observed their influence on the protective electron beam-induced

carbon layer. It should be noted that the heating holder for the ETEM experiments required TEM grids with a holey carbon support film. No changes were observed in the aspect ratio of the Au NRs during heating up to 400°C with one hour dwell time at each 100°C step when N₂ or CO gases were introduced into the ETEM (Supporting Figure S4). Instead, it was revealed that the carbon layer thickness tended to increase as the experiment progressed, reaching almost double the initial value. The increase was more pronounced for the experiments performed under CO gas, where the carbon layer thickness of 1.5 nm, observed at the room temperature, increased to 3.7 nm at 400°C (Supporting Figure S4b and S5). It seems that besides the instant transformation of CTAB surrounding the Au NRs into an amorphous carbon layer, redistribution of carbonaceous species from other areas or from the carbon substrate continued during the heating experiments, and that this additional carbon formation was particularly promoted by the presence of CO gas.

As expected, under an oxygen atmosphere, the carbon layer was oxidized and the Au NRs became free to deform. Fig. 5 shows the results of the ETEM experiments, involving thermal treatment of Au NRs under mixed N₂/O₂ (1:1) and CO/O₂ (1:1) atmospheres, and under a pure O₂ atmosphere at different pressures. In the case of O₂ (Fig. 5b), slight deformation of the Au NRs was observed at 200°C along with a reduced thickness of the carbon layer surrounding it. At 400°C the carbon layer was completely gone and the Au particles deformed losing their anisotropic character. The impact of an oxidative environment is even more obvious from Supporting Movie 1, which shows that after heating the Au NRs under N₂ to 400°C with a heating rate of 10°C min⁻¹, and upon switching from a N₂ to an O₂ flow, the carbon layer disappeared within 1 min while a single Au NR was observed to deform during the following 4 min. In the presence of CO/O₂ (Fig. 5a), the observed deformation process was clearly slower, leading to a change in the Au NR aspect ratio from 3.5 to 2.2 after heating at 400°C for 60 min. The difference in the deformation rate appeared to be independent of the relative pressure of O₂, but rather related to the presence of CO which, as discussed above, seemed to promote deposition of carbonaceous species and thus replenishing the carbon layer that was being removed by oxidation (Fig. 5c, Supporting Figure S5).

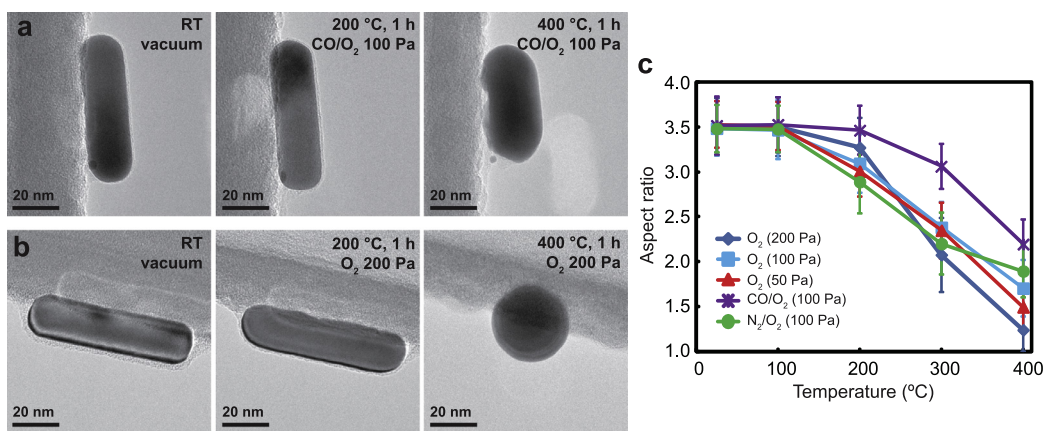


Fig. 5. ETEM results showing deformation of the Au NRs after 1 h heating at 200 °C and 400 °C under mixed CO/O₂ (100 Pa) atmosphere (a) and under pure O₂ (200 Pa) atmosphere (b). Dependence of the Au NR aspect ratio on the temperature under different gas atmospheres (c). Each point in (c) is the average value of the aspect ratio for more than 20 Au nanoparticles, and the standard deviation is indicated by bars.

Although the in-situ and ETEM experiments were performed at different acceleration voltages (120 kV and 200 kV, respectively) due to microscope limitations, we do not expect a different interaction of the probe electrons with the CTAB layer due to the following reasons. The two main mechanisms that lead to restructuring of organic material in a TEM are knock-on displacement and radiolysis. The knock-on threshold energy for organic bonds such as C-C or C-H is below 100 keV [44]. However, for organic materials the time between damage events is much longer than the time it takes to form the carbon layer. For example, on average it takes almost 100 min to break a C-H bond by knock-on damage while we observed that the formation of the amorphous carbon layer happened almost instantly [44]. Thus, knock-on displacement is unlikely to be the reason for the restructuring of the CTAB layer and should be comparable for both acceleration voltages. Radiolysis is the main damage mechanism for organic materials and is expected to be responsible for the restructuring of the CTAB layer. Since the signal/damage ratio is independent on the energy of the probe electrons for radiolysis [45], we do not expect a difference between the two acceleration voltages used which is confirmed by our experiments. Heating due to the electron beam can be excluded as it was recently calculated to lead to small temperature increases (2 K for Au NPs of about 10 nm) [44].

During the ex-situ experiments presented in Fig. 1 we observed that the Au NRs started to reshape at 100 °C in the presence of air and fully deformed during heating at 200 °C for 1 h. During the in-situ ETEM experiments, the Au NR did not deform when heated at 200 °C for 1 h but 400 °C was needed to achieve a full deformation to a spherical shape (Fig. 5b). This difference could stem from the large difference in oxygen pressure for these two experiments. Even though it was shown that the rate of deformation is independent of O₂ pressure for the in-situ experiments (Fig. 5c), there was 2–3 orders of magnitude more oxygen present when the sample was heated ex-situ at atmospheric pressure in air. However, it also needs to be considered that for the in-situ ETEM experiments an amorphous carbon layer was present as opposed to a CTAB layer when the particles were heated in air. Thus, these two reaction pathways are different. In any case we have shown that to understand in-situ processes it is not only important to analyze the influence of the electron beam but also how different environmental conditions change the outcome of the results. While electron microscopy experiments are generally performed under high vacuum conditions, our results highlight that it is important to compare the outcome of the experiment under different conditions such as gases and pressures to check if results may be different from those under realistic conditions.

4. Conclusions

While studying the thermal stability of CTAB-coated Au NRs in-situ in an electron microscope, we observed that the electron beam had a

tremendous impact on the outcome of the experiments. Due to electron beam irradiation a protective carbon layer was formed by almost instant (with respect to the time scale of the particle deformation) pyrolysis of the CTAB surfactant surrounding the Au NRs. The particles surrounded by such a carbon layer did not deform in inert atmospheres, even at temperatures as high as 400 °C. When the carbon coated Au NRs were exposed to an oxidizing environment while heating in an environmental TEM, the protective carbon layer was gradually removed and the surface gold atoms were free to migrate resulting in NR deformation towards spherical shapes. Ex-situ heating experiments in a static air oven revealed that the same NRs deformed to spherical shapes when heated at 200 °C for 1 h. Given the large discrepancy between the obtained stabilities during in-situ and ex-situ experiments, the electron beam influence cannot be neglected during such studies. Therefore, in order to avoid misinterpretation, in-situ TEM investigations need to be critically assessed and compared to data obtained from ex-situ experiments.

Acknowledgments

The authors thank the support of J. D. Meeldijk and C. Schneijdenberg with the TEM in-situ heating measurements at Utrecht University. A. van de Glind is grateful for the financial support granted by the Focus and Mass project of Utrecht University. The authors would also like to thank M. A. van Huis for providing the in-situ TEM heating stage equipment. A part of this work was supported by Program for Advancing Strategic International Networks to Accelerate the Circulation of Talented Researchers by JSPS. The research leading to these results has received funding from the European Research Council, Seventh Framework Programme (FP-2007-2013)/ERC Advanced Grant Agreement no. 338846 and no. 291667 HierarSACol.

Supplementary material

Supplementary material associated with this article can be found, in the online version, at doi:10.1016/j.ultramic.2018.05.006.

References

- [1] H. Takahashi, Y. Niidome, S. Yamada, Controlled release of plasmid DNA from gold nanorods induced by pulsed near-infrared light. *Chem. Commun.* (2005) 2247–2249, <http://dx.doi.org/10.1039/b500337g>.
- [2] Z. Zhang, L. Wang, J. Wang, X. Jiang, X. Li, Z. Hu, Y. Ji, X. Wu, C. Chen, Mesoporous silica-coated gold nanorods as a light-mediated multifunctional theranostic platform for cancer treatment, *Adv. Mater.* 24 (2012) 1418–1423, <http://dx.doi.org/10.1002/adma.201104714>.
- [3] P.K. Sudeep, S.T.S. Joseph, K.G. Thomas, Selective detection of cysteine and glutathione using gold nanorods, *J. Am. Chem. Soc.* 127 (2005) 6516–6517.
- [4] C.-Z. Li, K.B. Male, S. Hrapovic, J.H.T. Luong, Fluorescence properties of gold nanorods and their application for DNA biosensing. *Chem. Commun.* (2005) 3924–3926, <http://dx.doi.org/10.1039/b504186d>.

- [5] R.A. Alvarez-Puebla, A. Agarwal, P. Manna, B.P. Khanal, P. Aldeanueva-Potel, E. Carbó-Argibay, N. Pazos-Pérez, L. Vigdeman, E.R. Zubarev, N.A. Kotov, L.M. Liz-Marzán, Gold nanorods 3D-supercrystals as surface enhanced raman scattering spectroscopy substrates for the rapid detection of scrambled prions. *PNAS* 108 (2011) 8157–8161, <http://dx.doi.org/10.1073/pnas.1016530108>.
- [6] S.T. Sivapalan, B.M. Devetter, T.K. Yang, T.V. Dijk, M.V. Schulmerich, P.S. Carney, R. Bhargava, C.J. Murphy, Off-resonance surface-enhanced raman spectroscopy from gold nanorod suspensions as a function of aspect ratio: not what we thought, *ACS Nano* 7 (2013) 2099–2105.
- [7] S. Linić, U. Aslam, C. Boerigter, M. Morabito, Photochemical transformations on plasmonic metal nanoparticles, *Nat. Mater.* 14 (2015) 567–576, <http://dx.doi.org/10.1038/nmat4281>.
- [8] P. Zijlstra, J.W.M. Chon, M. Gu, Five-dimensional optical recording mediated by surface plasmons in gold nanorods. *Nature* 459 (2009) 410–413, <http://dx.doi.org/10.1038/nature08053>.
- [9] M. Mansuripur, A.R. Zakharian, A. Lesuffleur, S.-H.H. Oh, R.J. Jones, N.C. Lindquist, H. Im, A. Kobayakov, J.V. Moloney, Plasmonic nano-structures for optical data storage. *Opt. Express* 17 (16) (2009) 14001–140014, <http://dx.doi.org/10.1364/OE.17.014001>.
- [10] A.B. Taylor, J. Kim, J.W.M. Chon, Detuned surface plasmon resonance scattering of gold nanorods for continuous wave multilayered optical recording and readout, *Opt. Express* 20 (2012) 5069–5081, <http://dx.doi.org/10.1364/OE.20.005069>.
- [11] A. Ullah, X. Li, X. Cheng, X. Hao, Y. Su, J. Ma, M. Gu, Low energy-density recording with a high-repetition-rate laser beam in gold-nanorod-embedded discs, *Opt. Express* 20 (2012) 2362–2368.
- [12] L.C. Kennedy, L.R. Bickford, N.A. Lewinski, A.J. Coughlin, Y. Hu, E.S. Day, J.L. West, R.A. Drezek, A new era for cancer treatment: gold-nanoparticle-mediated thermal therapies, *Small* 7 (2011) 169–183, <http://dx.doi.org/10.1002/sml.201000134>.
- [13] Y. Akiyama, T. Mori, Y. Katayama, T. Niidome, Conversion of rod-shaped gold nanoparticles to spherical forms and their effect on biodistribution in tumor-bearing mice, *Nanoscale Res. Lett.* 7 (2012) 565, <http://dx.doi.org/10.1186/1556-276X-7-565>.
- [14] X.H. Huang, I.H. El-Sayed, W. Qian, M.A. El-Sayed, Cancer cell imaging and photothermal therapy in the near-infrared region by using gold nanorods, *J. Am. Chem. Soc.* 128 (2006) 2115–2120, <http://dx.doi.org/10.1021/ja057254a>.
- [15] W. Ni, X. Kou, Z. Yang, J. Wang, Tailoring longitudinal surface plasmon wavelengths, scattering and absorption cross sections of gold nanorods, *ACS Nano* 2 (2008) 677–686, <http://dx.doi.org/10.1021/nn7003603>.
- [16] C.J. Murphy, T.K. Sau, A.M. Gole, C.J. Orendorff, J. Gao, L. Gou, S.E. Hunyadi, T. Li, Anisotropic metal nanoparticles: synthesis, assembly, and optical applications, *J. Phys. Chem. B* 109 (2005) 13857–13870, <http://dx.doi.org/10.1021/jp0516846>.
- [17] Y. Liu, E.N. Mills, R.J. Composto, Tuning optical properties of gold nanorods in polymer films through thermal reshaping, *J. Mater. Chem.* 19 (2009) 2704–2709, <http://dx.doi.org/10.1039/b901782h>.
- [18] C.M. Tollan, R. Marcilla, J.A. Pomposo, J. Rodriguez, J. Aizpurua, J. Molina, D. Meecerreyes, Irreversible thermochromic behavior in gold and silver nanorod/polymeric ionic liquid nanocomposite films, *ACS Appl. Mater. Interfaces* 1 (2009) 348–352, <http://dx.doi.org/10.1021/am800058x>.
- [19] W.J. Kennedy, K.A. Slinker, B.L. Volk, H. Koerner, T.J. Godar, G.J. Ehlert, J.W. Baur, High-resolution mapping of thermal history in polymer nanocomposites: gold nanorods as microscale temperature sensors, *ACS Appl. Mater. Interfaces* 7 (2015) 27624–27631, <http://dx.doi.org/10.1021/acsami.5b08188>.
- [20] M.B. Mohamed, K.Z. Ismail, S. Link, M.A. El-Sayed, Thermal reshaping of gold nanorods in micelles, *J. Phys. Chem. B* 102 (1998) 9370–9374, <http://dx.doi.org/10.1021/jp9831482>.
- [21] H. Petrova, J. Perez Juste, I. Pastoriza-Santos, G.V. Hartland, L.M. Liz-Marzán, P. Mulvaney, On the temperature stability of gold nanorods: comparison between thermal and ultrafast laser-induced heating. *Phys. Chem. Chem. Phys.* 8 (2006) 814–821, <http://dx.doi.org/10.1039/b514644e>.
- [22] Y. Khalavka, C. Ohm, L. Sun, F. Banhart, C. Sönnichsen, Enhanced thermal stability of gold and silver nanorods by thin surface layers, *J. Phys. Chem. C* 111 (2007) 12886–12889, <http://dx.doi.org/10.1021/jp075230f>.
- [23] A. Antonello, E. Della Gaspera, J. Baldauf, G. Mattei, A. Martucci, Improved thermal stability of Au nanorods by use of photosensitive layered titanates for gas sensing applications, *J. Mater. Chem.* 21 (2011) 13074–13078, <http://dx.doi.org/10.1039/c1jm12537k>.
- [24] S.P.O. Danielsen, J. Choi, R.J. Composto, Retardation of shape change of Au nanorods using photo-cross-linkable ligands, *J. Polym. Sci. Part B Polym. Phys.* 54 (2016) 301–307, <http://dx.doi.org/10.1002/polb.23929>.
- [25] W. Albrecht, T.-S. Deng, B. Goris, M.A. van Huis, S. Bals, A. van Blaaderen, Single particle deformation and analysis of silica-coated gold nanorods before and after femtosecond laser pulse excitation, *Nano Lett.* 16 (2016) 1818–1825, <http://dx.doi.org/10.1021/acs.nanolett.5b04851>.
- [26] Y. Kuwauchi, H. Yoshida, T. Akita, M. Haruta, S. Takeda, Intrinsic catalytic structure of gold nanoparticles supported on TiO₂, *Angew. Chemie Int. Ed.* 51 (2012) 7729–7733, <http://dx.doi.org/10.1002/anie.201201283>.
- [27] T. Uchiyama, H. Yoshida, Y. Kuwauchi, S. Ichikawa, S. Shimada, M. Haruta, S. Takeda, Systematic morphology changes of gold nanoparticles supported on CeO₂ during CO oxidation, *Angew. Chemie Int. Ed.* 50 (2011) 10157–10160, <http://dx.doi.org/10.1002/anie.201102487>.
- [28] P.L. Hansen, J.B. Wagner, S. Helveg, J.R. Rostrup-Nielsen, B.S. Clausen, H. Topsøe, Atom-resolved imaging of dynamic shape changes in supported copper nanocrystals, *Science* 295 (2002) 2053–2055, <http://dx.doi.org/10.1126/science.1069325>.
- [29] T.W. Hansen, J.B. Wagner, P.L. Hansen, S. Dahl, H. Topsøe, C.J.H. Jacobsen, Atomic-resolution in situ transmission electron microscopy of a promoter of a heterogeneous catalyst, *Science* 294 (2001) 1508–1510, <http://dx.doi.org/10.1126/science.1064399>.
- [30] R.F. Egerton, P. Li, M. Malac, Radiation damage in the TEM and SEM, *Micron* 35 (2004) 399–409, <http://dx.doi.org/10.1016/j.micron.2004.02.003>.
- [31] R. Sarkar, C. Rentenberger, J. Rajagopalan, Electron beam induced artifacts during in situ TEM deformation of nanostructured metals, *Sci. Rep.* 5 (2015) 16345, <http://dx.doi.org/10.1038/srep16345>.
- [32] A.L. Koh, E. Gidcumb, O. Zhou, R. Sinclair, Oxidation of carbon nanotubes in an ionizing environment, *Nano Lett.* 16 (2016) 856, <http://dx.doi.org/10.1021/acs.nanolett.5b03035>.
- [33] H. Yoshida, H. Omote, S. Takeda, Oxidation and reduction processes of platinum nanoparticles observed at the atomic scale by environmental transmission electron microscopy, *Nanoscale* 6 (2014) 13113–13118.
- [34] N.M. Schneider, M.M. Norton, B.J. Mendel, J.M. Grogan, F.M. Ross, H.H. Bau, Electron - Water interactions and implications for liquid cell electron microscopy, *J. Phys. Chem. C* 118 (2014) 22373–22382.
- [35] A. Guerrero-Martínez, J. Pérez-Juste, E. Carbó-Argibay, G. Tardajos, L.M. Liz-Marzán, Gemini-surfactant-directed self-assembly of monodisperse gold nanorods into standing superlattices, *Angew. Chemie Int. Ed.* 48 (2009) 9484–9488, <http://dx.doi.org/10.1002/anie.200904118>.
- [36] S. Takeda, H. Yoshida, Atomic-resolution environmental TEM for quantitative in situ microscopy in materials science, *J. Electron Microsc.* 62 (2013) 193–203, <http://dx.doi.org/10.1093/jmicro/dfs096>.
- [37] R. Kumar, H.-T. Chen, J.L.V. Escoto, V.S.-Y. Lin, M. Pruski, Template removal and thermal stability of organically functionalized mesoporous silica nanoparticles, *Chem. Mater.* 18 (2006) 4319–4327.
- [38] B. Nikoobakht, M.A. El-Sayed, Evidence for bilayer assembly of cationic surfactants on the surface of gold nanorods, *Langmuir* 17 (2001) 6368–6374, <http://dx.doi.org/10.1021/la010530o>.
- [39] W. Ding, D.A. Dikin, X. Chen, R.D. Piner, R.S. Ruoff, E. Zussman, X. Wang, X. Li, Mechanics of hydrogenated amorphous carbon deposits from electron-beam-induced deposition of a paraffin precursor, *J. Appl. Phys.* 98 (2005) 014905, <http://dx.doi.org/10.1063/1.1940138>.
- [40] M.A. Baker, Plasma cleaning and the removal of carbon from metal surfaces, *Thin Solid Films* 69 (1980) 359–368.
- [41] M.A. Asoro, D. Kovar, P.J. Ferreira, Effect of surface carbon coating on sintering of silver nanoparticles: in situ TEM observations, *Chem. Commun.* 50 (2014) 4835–4838, <http://dx.doi.org/10.1039/c4cc01547a>.
- [42] M.A. Asoro, P.J. Ferreira, D. Kovar, In situ transmission electron microscopy and scanning transmission electron microscopy studies of sintering of Ag and Pt nanoparticles, *Acta Mater.* 81 (2014) 173–183, <http://dx.doi.org/10.1016/j.actamat.2014.08.028>.
- [43] A.B. Taylor, A.M. Siddiquee, J.W.M. Chon, Below melting point photothermal reshaping of single gold nanorods driven by surface diffusion, *ACS Nano* 8 (2014) 12071–12079.
- [44] J.C. Azcárate, M.H. Fonticelli, E. Zelaya, Radiation damage mechanisms of monolayer-protected nanoparticles via TEM analysis, *J. Phys. Chem. C* 121 (2017) 26108–26116, <http://dx.doi.org/10.1021/acs.jpcc.7b08525>.
- [45] R. Egerton, Mechanisms of radiation damage in beam-sensitive specimens, for TEM accelerating voltages between 10 and 300 kv, *Microsc. Res. Tech.* 75 (2012) 1550–1556.